Toxicology in Vitro 82 (2022) 105373

Contents lists available at ScienceDirect

Toxicology in Vitro

journal homepage: www.elsevier.com/locate/toxinvit

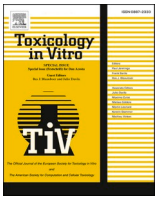

Estrogen treatment reduced oxalate transporting activity and enhanced migration through the involvement of SLC26A6 in lung cancer cells

Dongun Lee [a], Peter Chang-Whan Lee [b], Jeong Hee Hong [a,*], Dong Min Shin [c,*]

[a] Department of Health Sciences and Technology, Lee Gil Ya Cancer and Diabetes Institute, GAIHST, Gachon University, 155 Getbeolro, Yeonsu-gu, Incheon 21999, Republic of Korea
[b] Department of Biomedical Sciences, University of Ulsan College of Medicine, Asan Medical Center, Seoul, Republic of Korea
[c] Department of Oral Biology, BK21 PLUS Project, College of Dentistry, Yonsei University, Seoul, Republic of Korea

ARTICLE INFO

Editor: P Jennings

Keywords:
Estrogen
Chloride bicarbonate exchanger
Oxalate transporter
Internalization
Lung cancer

ABSTRACTS

Estrogen therapy has used to prevent bone loss in postmenopausal women. Although therapeutically enhanced estrogen levels have been suggested, patients are exposed to greater risks of nephrolithiasis and cancer. It has been known that oxalate or bicarbonate transporter SLC26A6 is involved in oxalate homeostasis and its deletion results in kidney stone formation and addressed that patients with kidney stones possess higher cancer risk. Thus, the mechanism of the interaction between estrogen and SLC26A6 and the effect of SLC26A6 on cancer cells should be elucidated. In this study, we investigated whether β-estradiol treatment modulates SLC26A6 expression and its bicarbonate or oxalate transporting activity and affects the proliferative and migratory ability of A549 cells. The β-estradiol stimulation attenuated oxalate or bicarbonate transporting activities through SLC26A6. Knockdown of SLC26A6 reduced transporter activity whereas enhanced cellular migration. β-estradiol-mediated cellular migration was independent of SLC26A6 transporter activity, whereas enhanced SLC26A6 expression attenuated cellular migration even in the presence of β-estradiol treatment. These results indicate β-estradiol treatment enhances cancer cell migration and dysregulates oxalate transport by inhibiting SLC26A6 activity, suggesting reduced oxalate transporting activity may involve in the oxalate homeostasis.

1. Introduction

Estrogen hormone replacement therapy (HRT) has been recommended to treat osteoporosis in postmenopausal women (Dawson-Hughes et al., 1990; Domrongkitchaiporn et al., 2002). Although estrogen therapy has been positively addressed in bone biology, HRT has been linked with an enhanced potential risk of nephrolithiasis or conversely reduced deposition of renal calcium-oxalate crystals (Fan et al., 1999; Heller et al., 2002; Maalouf et al., 2010; Peerapen and Thongboonkerd, 2019). HRT enhances serum 1,25-dihydroxyvitamin D3 level and subsequently enhances high calcium level in urine (van Hoof et al., 1994). In addition, high serum estrogen levels induced by HRT are related to the development and malignancy of cancers accompanying with reduction of DNA repair rate, poor survival rate in lung cancer, and increase of aromatase level (Chakraborty et al., 2010; Liang and Shang, 2013; Rodriguez-Lara et al., 2018; Rothenberger et al., 2018). Large scale population-based cohort study has been reported that patients with kidney stones are at higher cancer risk in various systemic cancers such as lung, bladder, thyroid, head and neck, breast, and urinary cancer (Shih et al., 2014). Cancer and nephrolithiasis are complex factor-derived processes. High calcium level in serum caused by HRT is not always associated with incidence of kidney stone formation (Domrongkitchaiporn et al., 2002). Otherwise, it appears that although elevated estrogen levels are therapeutically beneficial, patients with HRT are exposed to the potential risk of nephrolithiasis and cancer.

The kidney stone-associated transporter chloride/bicarbonate (Cl^-/HCO_3^-) exchanger (CBE) solute carrier family 26 member 6 (SLC26A6, abbreviated to A6) is mainly identified in secretory glands such as salivary gland ducts (Lee et al., 2012b), pancreas (Wang et al., 2006), and intestine (Singh et al., 2008) and is responsible for bicarbonate ion secretion. Its bicarbonate transporting function is also associated with cardiac function and the maintenance of pH homeostasis (Alvarez et al., 2004; Sirish et al., 2017). A6 is also well known to act as a chloride/oxalate exchanger (COE) in intestine (Freel et al., 2006; Jiang et al., 2006) and kidneys (Freel et al., 2006) to regulate oxalate homeostasis. The bicarbonate transport function of A6 is considered to regulate

* Corresponding authors.
E-mail addresses: minicleo@gachon.ac.kr (J.H. Hong), dmshin@yuhs.ac (D.M. Shin).

https://doi.org/10.1016/j.tiv.2022.105373
Received 30 January 2022; Received in revised form 19 April 2022; Accepted 26 April 2022
Available online 29 April 2022

intracellular pH and anion transport in epithelial cells. Insoluble calcium oxalate crystals have been considered as one of component of kidney stone and level of serum oxalate is associated with kidney stone. A6 also transports oxalate and is related to oxalate transport, involved in intestinal oxalate secretion and nephrolithiasis (Amin et al., 2018; Khamaysi et al., 2019; Ohana et al., 2013). In *ob* mice, obesity-associated hyperoxaluria was induced by reducing *Slc26a6* gene expression (Amin et al., 2018), and in *Slc26a6*-null mice oxalate secretion was reduced, and plasma oxalate levels were elevated (Garcia-Perez et al., 2012). Although oxalate transporting role of A6 has been addressed in various studies, the regulatory mechanisms on A6 are relatively undefined.

In a previous study, it was reported that estrogen and estrogen receptor (ESR) contribute to lung cancer activation (Hsu et al., 2017). In another, estradiol treatment promoted lung cancer cell migration by stimulating the CXCL12/CXCR4 pathway (Rodriguez-Lara et al., 2017). Although A6 is ubiquitously expressed, no disease-related human mutation of A6 has yet been discovered (Wang et al., 2020). More recently, enhanced expression of A6 is demonstrated in hepatocellular carcinoma (Zhu et al., 2021). These evidences conduct that relationship between estrogen and A6 should be elucidated in cancer biology and oxalate homeostasis. Thus, we hypothesized that enhanced estrogen level reflects increased incidence of cancer and modulates oxalate homeostasis and evaluate the effect of estrogen on oxalate transporter.

In this study, we speculated that estrogen-mediated intensive symptoms including oxalate homeostasis and lung cancer activation are related to A6 expression or A6-mediated ion transporting activity. Thus, we examined two aspects of the activities of A6, that is, as an ion transporter for cellular migration (Schwab et al., 2012) and as an oxalate transporter for oxalate homeostasis, by treating A549 (a lung adenocarcinoma cell line) cells (an A6 expressing lung cancer cell line) with β-estradiol (β-E2). In addition, we investigated whether β-E2 modulates A6 expression and transporting activity and affects the proliferative and migratory ability of A549 cells.

2. Material and methods

2.1. Reagents and cell culture

β-E2 was purchased from Sigma. A549 cells, and a human embryonic kidney 293 T cell line (H.T) were obtained from ATCC. The maintenance of the cells was proceeded with Dulbecco's Modified Eagle's Medium (DMEM, Thermo) in the presence of FBS (10%, Invitrogen) with penicillin/streptomycin (Invitrogen) in a humidified CO_2 (5%) incubator at 37 °C. When cells confluence reached to 80% density, trypsin/ethylenediaminetetraacetic acid (EDTA) was treated with to detach the cells. The detached cells were put onto new culture dishes for all experiments except for live-cell imaging which using coverslips in culture dishes.

2.2. Plasmids, small interfering RNA (siRNA), and transfections

The complementary DNA (cDNA) encoding SLC26A6 (*A6*) was cloned in eGFP-C1, and STE20/SPS1-related proline-alanine-rich protein kinase (SPAK) or SPAK dominant negative (DN) were constructed in p3XFLAG-CMV-7.1. The plasmids had been provided by Dr. Shmuel Muallem (National Institutes of Health, Bethesda, USA). The siRNA for *A6* was constructed using Double-Promoter pFIV-H1/U6 siRNA cloning vectors (System Biosciences), followed by the manufacturer's instructions. The vectors contained siRNA strands for human siRNA-A6 (siA6) (sense, 5′-AAA GGA AGC TGC CCC AGA GCA AGG TTG GC-3′, and anti, 5′-AAA GCC AAA CCT TGC TCT GGG GCA GCT TC-3′). Plasmids such as *A6* were transfected using jetPRIME Transfection Reagent (Polyplus-transfection) depending on the manufacturer's instructions. Each plasmid was mixed with jetPRIME buffer, and then transfection reagent was mixed. The transfecting solution was incubated at room temperature (RT) for 10 min. The incubated mixture transferred to A549 cells in fresh DMEM medium. After incubation for 6 h, media were replaced with new DMEM, and the cells were incubated until use.

2.3. Migration assay

Transwell-membrane migration, wound healing, and agarose spot assay was used for detecting the migratory ability of A549 cells. For Transwell migration assays, detached A549 cells in DMEM containing 1% FBS were placed in upper transwell membrane which of pore size is 8.0 μm. The bottom plates were filled with new media containing 10% FBS with incubation for 6 h. Membranes were then fixed with chilled methanol (−20 °C) for 1 min at −20 °C and stained with DAPI or crystal violet. After PBS washing, the membranes were stained with DAPI solution (1 μg/mL in distilled water (DW)) for 30 min at 37 °C or 0.25% crystal violet solution in DW (with 20% methanol) at room temperature in the dark for 10 min and performed DW washing three times. Transwell membranes were placed between slide glass and cover glass and confocal microscopy was proceeded with LSM 700 (Carl Zeiss) (for DAPI) or an inverted microscope (Olympus) equipped with Mosaic software (Opto Science) (for crystal violet). The intensities of the images obtained were measured by the Meta Morph system (Molecular Devices).

For wound healing assays, A549 cells were cultured until approximately 80% confluent, scratched with 10 μL pipette tips, and incubated with plasmids under indicated conditions for 48 h at 37 °C. The images were measured by using an inverted microscope (Olympus) equipped with Mosaic software. Migration ranges were calculated as distance of initially exposed range subtracted by cell-migrated range.

For agarose spot assays, 0.5% of agarose in physiological salt solution (PSS; previously described in (Lee et al., 2018)) was used, and the mixture was heated. And then the mixture spotted to dishes and allowed at 4 °C to cool for 8 min, as described previously (Vinader et al., 2011; Wiggins and Rappoport, 2010). A549 cells were put the dishes to adhere for 4 h and then replaced with a new culture media containing FBS (0.1%) with penicillin-streptomycin (100 U/mL) in DMEM. The incubation time is proceeded at 37 °C for 24 h. The images were obtained using Meta Morph software. Cells observed under agarose spots were counted as migrated cells.

2.4. MTT assay

β-E2 was treated to 5×10^3 number of A549 cells (per well) in 96-well plates. After indicated incubation times, tetrazolium bromide (1 mg/mL, Georgia Chemicals Inc.) solution was treated for 2 h at 37 °C. The cells were treated with DMSO to dissolve formazan crystals, and absorbances were analyzed with UVM 340 microplate reader (Biochrom) at 570 nm.

2.5. Cl^--HCO_3^- exchange (CBE) activity

The attached cells onto coverslips were stained with 6 μM BCECF-AM (2′, 7′-bis-(carboxyethyl)-5-(and-6)-carboxyfluorescein, TEFlabs) in the presence of 0.05% pluronic acid (BCECF-AM loading enhancer, Invitrogen) for 15 min at room temperature into perfusion chamber. The samples were allowed to flowing PSS for 4 min to wash. pH_i was analyzed by measuring dual excitatory wavelength of BCECF fluorescence (495 and 440 nm) to emit fluorescence at 530 nm. CBE activity was defined as the slope (changes of BCECF fluorescence intensity versus time) in the cells with CO_2-provided HCO_3^--buffered solution without chloride (previously described in (Lee et al., 2018)). Images were taken by a CCD camera (Retiga 6000, Q-Imaging) and analyzed using the Meta Fluor system (Molecular Devices).

2.6. Cl^--oxalate exchange (COE) activity

The attached cells onto coverslips were stained with 5 mM

ethoxycarbonylmethyl-6-methoxyquinolinium bromide (MQAE, Cayman Chemical) in the presence of 0.05% pluronic acid for 15 min at room temperature into perfusion chamber. The samples were allowed to flowing PSS for 4 min to wash. $[Cl^-]_i$ was analyzed by measuring excitatory wavelength of MQAE fluorescence (360 nm) to emit fluorescence at 530 nm. COE activity was defined as the slope (changes of MQAE fluorescence intensity versus time) in the cells with chloride-oxalate solution (Table 1). Images were obtained using a CCD camera and analyzed using the Meta Fluor system.

2.7. Na^+-H^+ exchanger (NHE) activity

The attached cells onto coverslips were stained with 6 μM BCECF-AM (TEFlabs) in the presence of 0.05% pluronic acid (Invitrogen) for 15 min at room temperature into perfusion chamber. The samples were allowed to flowing PSS for 4 min to wash. pH_i was analyzed by measuring dual excitatory wavelength of BCECF fluorescence (495 and 440 nm) to emit fluorescence at 530 nm. NHE activity defined as the slope (changes of BCECF fluorescence intensity versus time) was measured by the slope of increased intensity in the cells with PSS after NH_4Cl solution (previously described in (Evans and Turner, 1997; Worrell et al., 2004)) and $0Na^+$ (in the presence of amiloride) solutions (previously described in (Hong et al., 2015)). Images were obtained using a CCD camera and analyzed using the Meta Fluor system.

2.8. Na^+- HCO_3^- cotransporter (NBC) activity

The attached cells onto coverslips were stained with 6 μM BCECF-AM (TEFlabs) as described above. The samples were allowed to flowing PSS for 4 min to wash. pH_i was analyzed by measuring dual excitatory wavelength of BCECF fluorescence (495 and 440 nm) to emit fluorescence at 530 nm. NBC activity was defined as the slope of increased intensity in the cells with CO_2-provided HCO_3^--buffered solution (previously described in (Hong et al., 2015)) with NHE inhibitor 5-(N-ethyl-N-isopropyl)-amiloride (EIPA), as previously described in (Ji et al., 2017). Images were obtained with a CCD camera and analyzed using the Meta Fluor system.

2.9. pH calibration

BCECF fluorescence ratios were altered to actual pH units using calibration curves, as described by Lee et al. (Lee et al., 2018). Briefly, BCECF-loaded cells were incubated in a pH 5.5 calibration solution containing 20 μM nigericin (Sigma) for 10 min, and then re-incubated under the same conditions at pH 6.0–8.5 (previously described in (Lee et al., 2018)). pH values were determined using a pH calibration curve (Fig. S1) derived using the equation ($pH = pKa-\log((R_{max}-R)/R-R_{min})$) (pKa of BCECF; 6.97, R; BCECF ratio, R_{max}; maximum ratio, R_{min}; minimum ratio).

2.10. Western blotting

A549 cells incubated under indicated conditions were suspended with lysis buffer in the presence of protease inhibitor. After sonication, cells were spun down (11,000 ×*g* for 15 min at 4 °C). The quantification of protein quantity to 30 μg was determined using the Bradford assay (Bio-rad). The protein samples were loaded to SDS-PAGE followed by transfer to methanol soaked polyvinylidene difluoride (PVDF, Bio-rad) membranes, and then blocked with 5% skim milk in TBS-T (Tris-buffered saline containing 0.5% Tween-20) for 1 h. After blocking the membranes incubated with β-actin (Sigma), estrogen receptor α (ESRα, Abcam), estrogen receptor β (ESRβ, Abcam), or SLC26A6/Pat1 (A6, Abcam) antibodies for 12 h at 4 °C, and washed three times with TBS-T. Washed samples were then treated with horseradish peroxidase (HRP)-conjugated secondary antibodies, and the protein bands were detected using ECL solution (Thermo).

2.11. Real time qPCR (qPCR)

Before qPCR, cDNA was synthesized from mRNA of A549 cells. mRNA extraction was proceeded using the Hybrid RiboEx extraction system (Geneall) and reverse transcription premix (Bioneer, South Korea). The reverse transcription condition was 37 °C for 90 min and 95 °C 5 min. qPCR was performed using the QuantStudio 3 real-time PCR system (Thermo) and the PowerUp SYBR Green Master Mix (Thermo) depending on the manufacturer's protocol. PCR step was performed with cDNA, 1× master mix, dH_2O (up to 20 μL), and 1 μL of forward and reverse oligomer (10 pmol/μL) (*GAPDH*; F: 5'-GAC CTG ACC TGC CGT CTA GAA A-3′, R: 5'-CCT GCT TCA CCA CCT TCT TGA-3′, *A6*; F: 5'-CCT ATG CCC TTC TGC TCC AA-3′, R: 5′-GAG CCA GTC ACG CAC AGG AT-3′). The mRNA expression level of *A6* was normalized versus that of GAPDH.

2.12. Confocal microscopy

The *A6*-transfected A549 cells on coverslips were fixed for 10 min at −20 °C with chilled methanol (−20 °C). The cells were washed with PBS three times, and then mounted on slide glasses with Fluoromount-G containing 4′,6-diamidino-2-phenylindole (DAPI) (Electron Microscopy Sciences). Confocal microscopy images were obtained using an LSM 700 Zeiss confocal microscope (Carl Zeiss) equipped with ZEN software (Carl Zeiss).

2.13. Statistical analyses

Data obtained from the number of experiments are indicated as means ± standard error of means (SEMs). Statistical significance was determined by analysis of variance using one-way ANOVA (*$p < 0.05$, **$p < 0.01$, *** $p < 0.001$).

3. Results

3.1. β-E2 treatment attenuated COE activity in A549

To investigate the effect of β-E2 in oxalate transport in A549 cells, we measured COE activities (Mount and Romero, 2004) using the MQAE-quenching technique in A549 cells. The A549 cells were stimulated with the physiologic concentration of β-E2 within range of 0.1 to 10 nM to avoid impaired mitochondrial membrane potential by a high concentration of β-E2 (Celojevic et al., 2011). We chose 2 nM of β-E2 to stimulate A549. COE activity represents oxalate transporting activity through the changes of extracellular Cl^- level (Mukaibo et al., 2018). β-E2 treatment attenuated COE activity (Fig. 1A,B). Treatment with β-E2 also attenuated CBE activity in A549 lung cancer cells (Fig. S2A,B). To verify the A6-mediated COE and COE activities, the mRNA and protein levels of A6 were measured in the presence of β-E2. β-E2 treatment did not change the mRNA and protein expressions of A6 (Fig. 1C,D). We observed various band sizes of A6 that occurred in detecting the protein with western blot analysis as also addressed in (Thomson et al., 2016). In addition, the protein levels of the ESRα and ESRβ estrogen receptors were not changed by β-E2 stimulation (Fig. 1E-G). Furthermore, A549 cell viability was not affected by β-E2 (Fig. S3). These results show that β-E2 treatment attenuated COE and CBE activities in A549 lung cancer cells.

3.2. A6 modulated CBE and COE activities

The anion exchanger A6 exchanges Cl^- for HCO_3^-, oxalate, hydroxyl, or formate (Petrovic et al., 2008; Wang et al., 2005). According to types of organ, Cl^-/ HCO_3^- transporting of A6 is mainly identified in salivary and pancreatic secretion (Lee et al., 2012b; Wang et al., 2006) and Cl^-/oxalate transporting is verified in kidney (Wang et al., 2005). To confirm the effect of A6 on ion transporter activity, we used the

Table 1
Components of chloride-oxalate solution.

Components	Concentration (mM)
Sodium chloride (NaCl)	95
N-Methyl-D-Glucamine chloride (NMDG-Cl)	27
HEPES	10
Glucose	5
Potassium chloride (KCl)	4.3
Magnesium chloride ($MgCl_2$)	1
Sodium oxalate (Na_2Ox)	25
pH 7.4	
310 mOsm (adjusted with mannitol)	

knockdown with siRNA and A6-overexpressed system. We verified reduced A6 expression in siA6-treated A549 cells (Fig. 2A). The two types of A6 activities were evaluated by measuring CBE (Fig. 2B,C) and COE (Fig. 2D,E) values. The intracellular pH calibration curve is shown in Fig. S1. The knockdown of A6 inhibited CBE and COE activities (Fig. 2B-E), whereas these activities were 3 times higher in A6-overexpressed cells than in non-transfected controls (Fig. 2F-I). These results indicate CBE and COE activities are dependent on A6 expression.

3.3. A6 expression affected the cellular migration

The patients with metastatic cancer possess complication to survive due to the uncontrollable proliferation of cancer cells (Stoletov et al.,

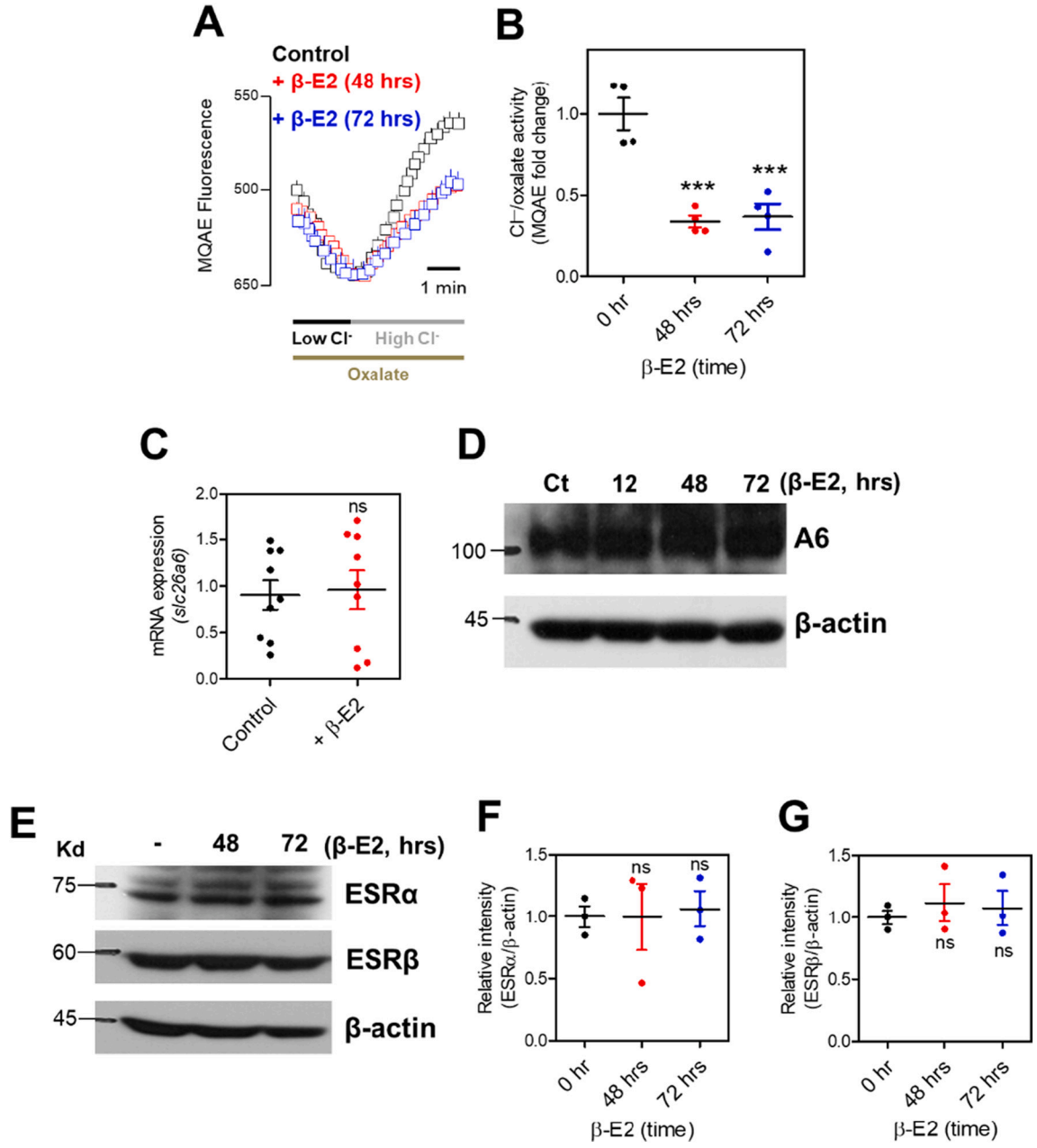

Fig. 1. β-E2 treatment attenuated COE activity in A549. (A) The COE activity in the presence of β-E2 treatment (2 nM, for 48 h-red; 72 h-blue) or in its absence (black) in A549 cells. (B) The graph indicates means ± SEMs of the number of experiments ($n = 4$, ***$p < 0.001$). (C) mRNA expressions of human *Slc26a6* as determined by qPCR. The graphs show the means ± SEMs of each relative expression ($n = 9$; ns = non-significant). (D) The western blotting of A6 with β-E2 treatment for 24, 48, and 72 h. (E) The western blotting of ESRα and ESRβ with β-E2 treatment for 48 and 72 h. (F, G) The graphs indicate means ± SEMs of the number of experiments ($n = 3$, ns = non-significant).

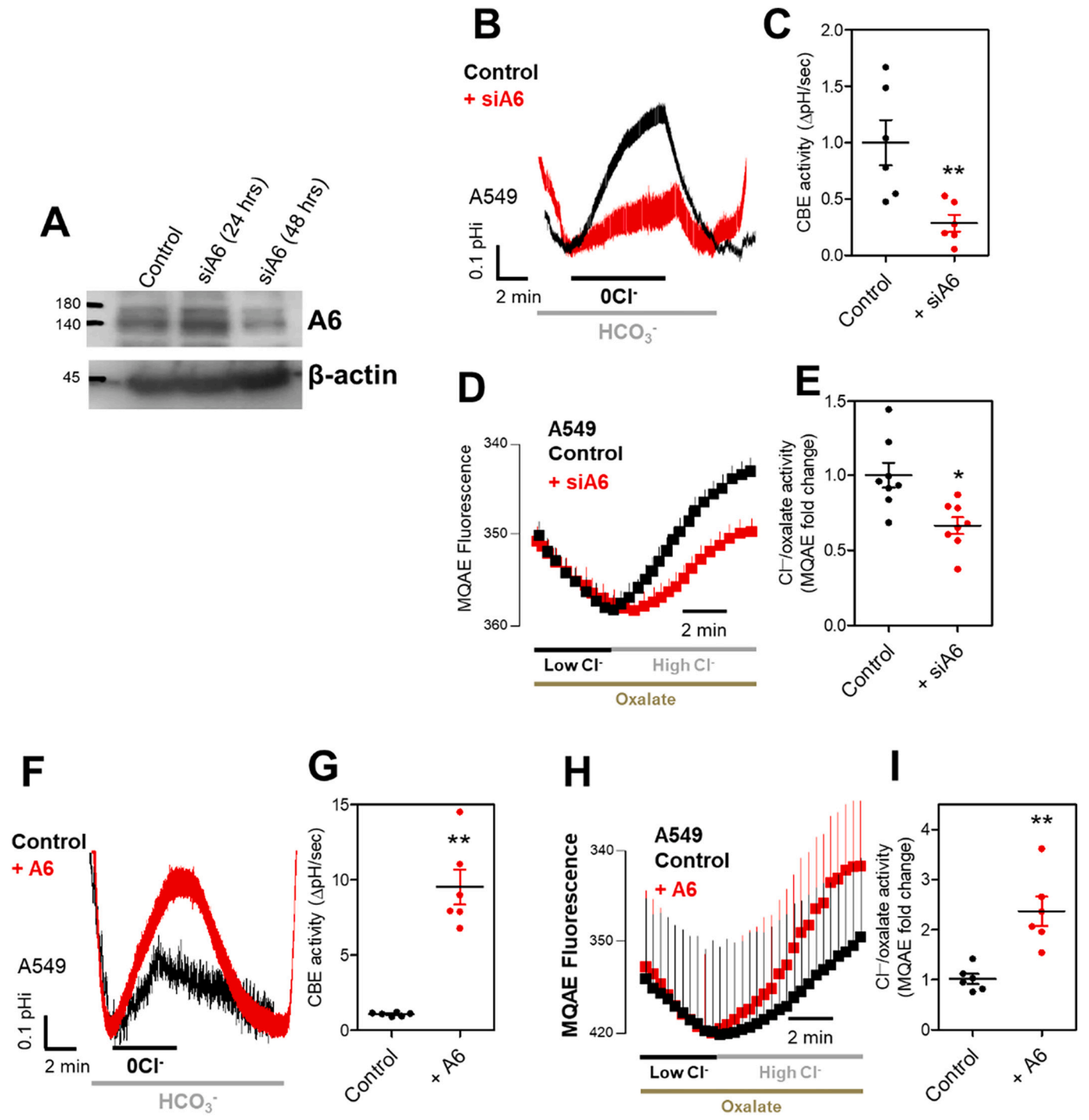

Fig. 2. A6 modulated CBE and COE activities. (A) Western blotting of A6 in siA6 transfected A549 cells. (B) The activity of CBE after A6 knockdown (red). (C) The graph shows means ± SEMs of relative CBE activities in A6 and SPAK-transfected A549 cells ($n = 6$, $^{**}p < 0.01$). (D) The activity of COE after A6 knockdown (red). (E) The graph shows means ± SEMs of relative COE activities ($n = 8$, $^{*}p < 0.05$). (F) The activity of CBE in cells overexpressing A6 (red). (G) The graph shows means ± SEMs of relative CBE activities (n = 6, $^{**}p < 0.01$). (H) Activity of COE in cells overexpressing A6 (red). (I) The graph shows means ± SEMs of relative COE activities (n = 6, $^{**}p < 0.01$). (For interpretation of the references to colour in this figure legend, the reader is referred to the web version of this article.)

2020). Thus, restriction of metastatic feature has been highlighted as a major point of cancer therapy. In other words, inhibition of cancer migration is a powerful cancer therapy not to spread cancer cells toward other tissues. In this section, we determined A549 migration through adjustment of A6 expression. β-E2 treatment did not reduce A6 expression in A549 cells, despite reducing CBE and COE activities. In a previous study, we showed HCO_3^--dependent transporters acts as an ion transporter for cellular migration including NBC (Hwang et al., 2021; Hwang et al., 2020b) and anion exchanger 2 (Hwang et al., 2019, 2020a). However, the relationship between A6 and cancer cell migration have not studied yet. Knockdown of *A6* enhanced cellular migration in the wound migration assay (Fig. 3A,B) but reduced CBE and COE activities. The specific antagonist or agonist for A6 activity has not been developed. Thus, to adjust activity of A6, SPAK was used. SPAK inhibits A6 activity by reducing its expression level through the phosphorylation of A6 in plasma membrane (Lee et al., 2012a). In the present study, H.T

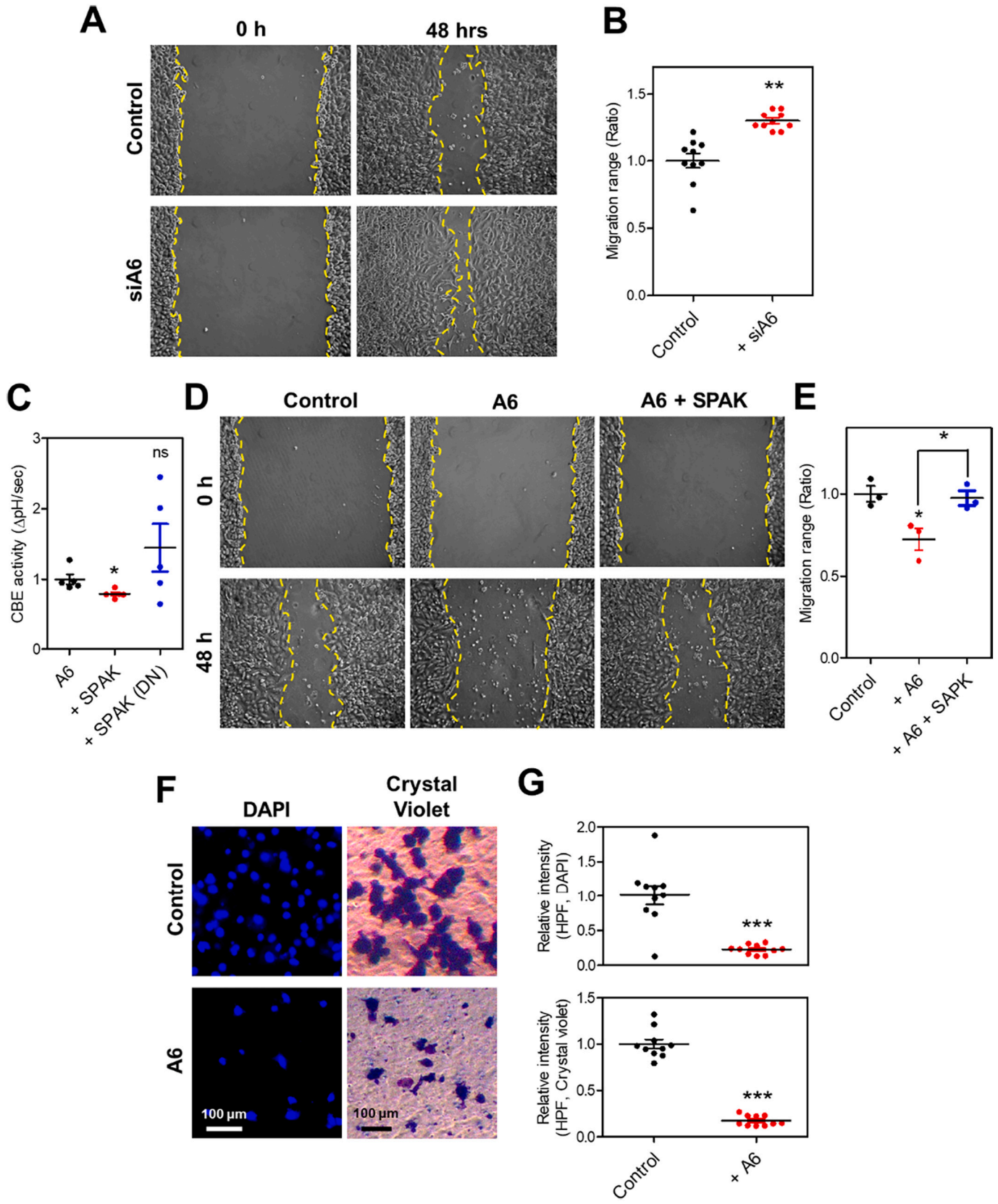

Fig. 3. Expression levels of A6 affected cellular migration. (A) The images show wound healing migration assay in siA6-transfected A549 cells. (B) The graphs indicate means ± SEMs of the migration range ($n = 10$, $^*p < 0.05$). (C) The graph show means ± SEMs of relative CBE activities ($n = 5$, *p < 0.05, ns = non-significant). (D) The images show the results of migration assays. (E) The graph indicate means ± SEMs of the migration range ($n = 3$, *p < 0.05). (F) Images showing transwell membranes containing cells transfected or not with A6 and stained with DAPI (blue) or crystal violet (purple). (G) The graphs indicate means ± SEMs of the relative intensities of DAPI and crystal violet staining (n = 10, $^{***}p < 0.001$). (For interpretation of the references to colour in this figure legend, the reader is referred to the web version of this article.)

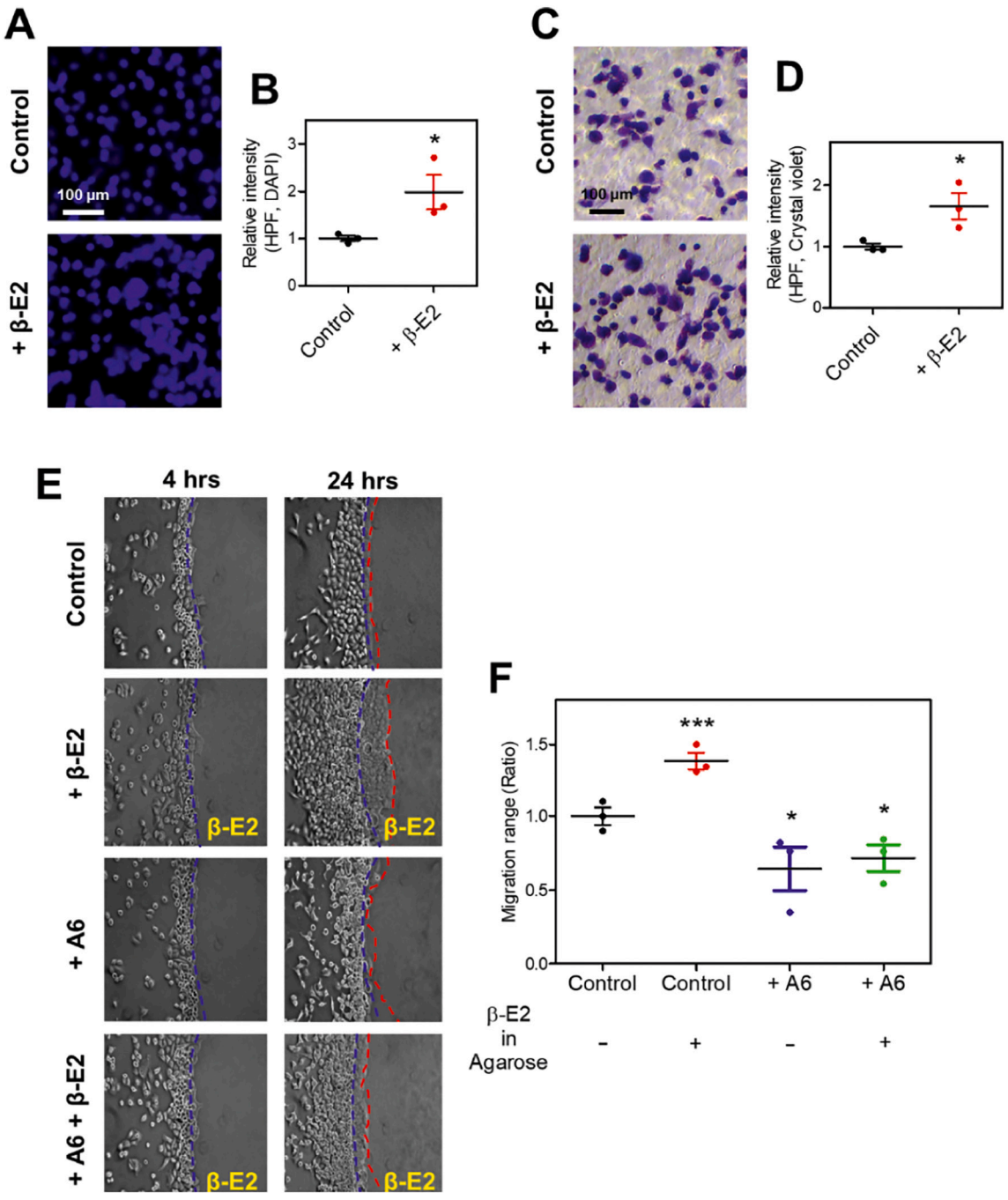

Fig. 4. β-E2 treatment enhanced cellular migration by modulating A6 expression. (A-D) Images of Transwell migration assay membranes stained with DAPI (blue) (A) or crystal violet (violet) (C). A549 cells were treated with 2 nM β-E2 for 72 h. Graphs were produced using the means ± SEMs of the relative intensities of DAPI (B) and crystal violet (D) staining (n = 3, *p < 0.05). (E) The images show agarose spot migration assay results obtained after incubating A549 cells for 4 h or 24 h under the indicated conditions. The dotted lines (blue) represent the initial boundary of the agarose spot (pH 7.5) and the red dotted lines represent the lineage of migrated cells into the agarose spots with and without β-E2 treatment. (F) Graph of means ± SEMs of migration ranges (n = 3, ***p < 0.001).

cells were transfected with SPAK or a DN form of SPAK in presence of A6. *SPAK* and *A6* co-transfected cells exhibited less CBE activity but not in cells transfected with the DN form of SPAK (Fig. 3C, Original traces are shown in Fig. S4). As regards the effects of A6 overexpression and knockdown on A549 migration, A6 overexpression reduced migration, whereas its knockdown enhanced migration (Fig. 3A,B). Presence of SPAK recovered migratory ability to control level as in knockdown of *A6* (Fig. 3D,E). To confirm the migratory role of A6 overexpression, transwell-membrane migration assay, composed of DAPI and crystal violet assay, was performed. The over-expression of A6 attenuated A549 cell migration (Fig. 3F,G). To investigate whether reduced cell viability affected cellular invasion, we performed agarose spot migration assays under A6-overexpressed conditions. We found that cellular invasion was reduced in A6-overexpressed A549 cells (Fig. S5). These results show A6 activity was not a dominant modulator of A549 migration but that the protein levels of A6 reduce A549 migratory activity.

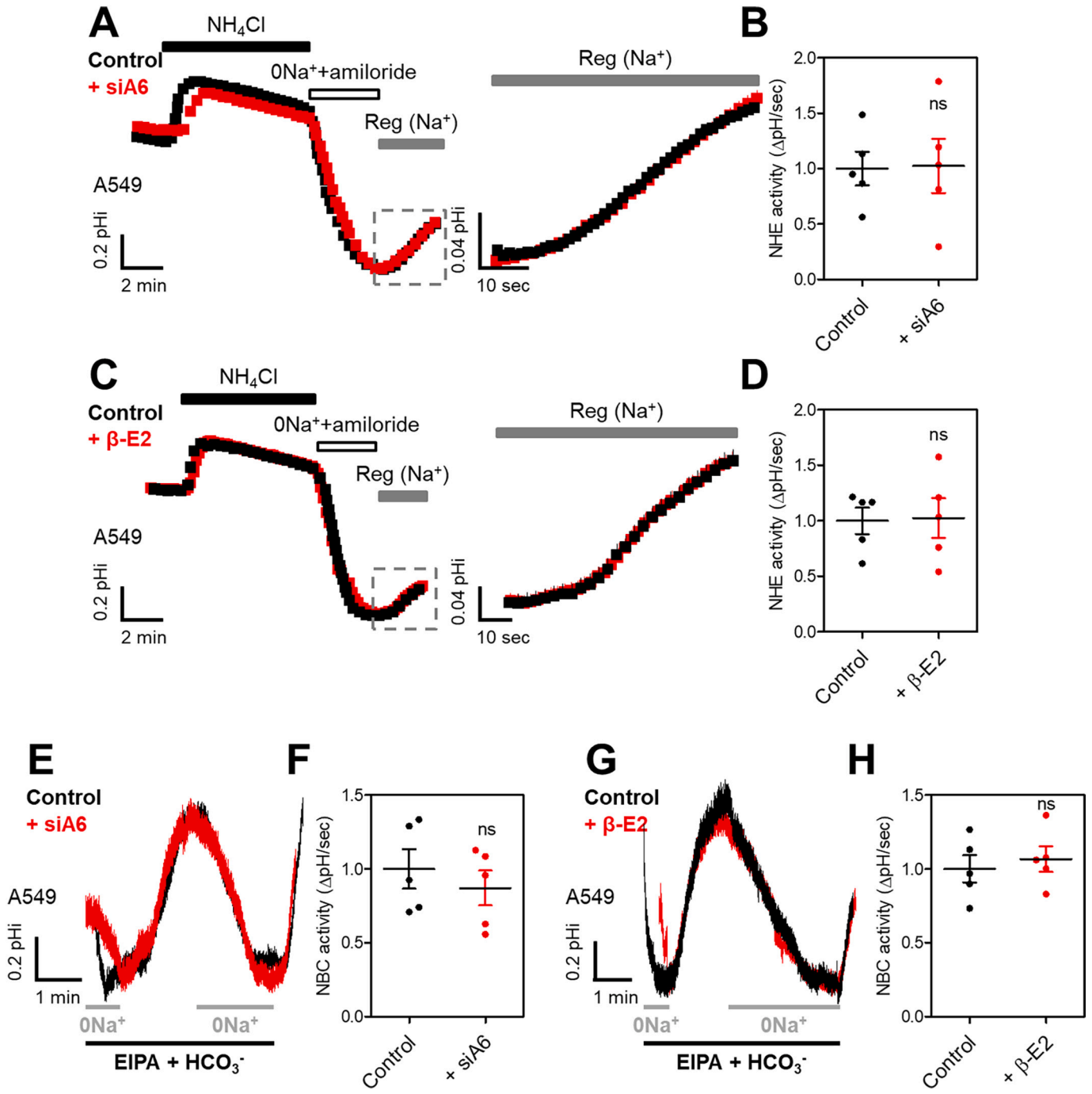

Fig. 5. NHE activity was independent of siA6- or β-E2 treatment – mediated migration. (A) The activities of $Na^+/K^+/Cl^-$ cotransporters (NKCC) or NHE after A6 knockdown (red). Right panel is a magnified trace of dotted square of left panel. (B) The graph shows the means ± SEMs of relative NHE activities ($n = 5$, ns = non-significant). (C) The activities of NKCC and NHE in A549 cells incubated with 2 nM β-E2 for 72 h (red). Right panel is a magnified trace of dotted square of left panel. (D) Graph of the means ± SEMs of relative NHE activities (n = 5, ns = non-significant). (E) Activities of NBC in siA6 transfected A549 cells (red). (F) The graph shows means ± SEMs of relative NBC activities (n = 5, ns = non-significant). (G) NBC activities in A549 cells incubated with β-E2 for 72 h (red). (H) Graph shows means ± SEMs of relative NBC activities (n = 5, ns = non-significant). (For interpretation of the references to colour in this figure legend, the reader is referred to the web version of this article.)

3.4. β-E2 treatment enhanced cellular migration by modulating A6 expression

It has been addressed that application of estrogen has been addressed lung cancer development (Chakraborty et al., 2010; Rodriguez-Lara et al., 2018). β-E2 treatment increased A549 cell migration as determined by transwell assay (Fig. 4A-D). We confirmed β-E2 treatment mediated migration using agarose spot assays. β-E2–containing agarose spot assays are efficient to determine the chemotaxis of β-E2 on A549 cells. A6 overexpression inhibited β-E2 treatment –mediated chemotaxis (Fig. 4E,F). These results indicate the presence of β-E2 treatment enhanced cellular migration, whereas A6 overexpression attenuated this

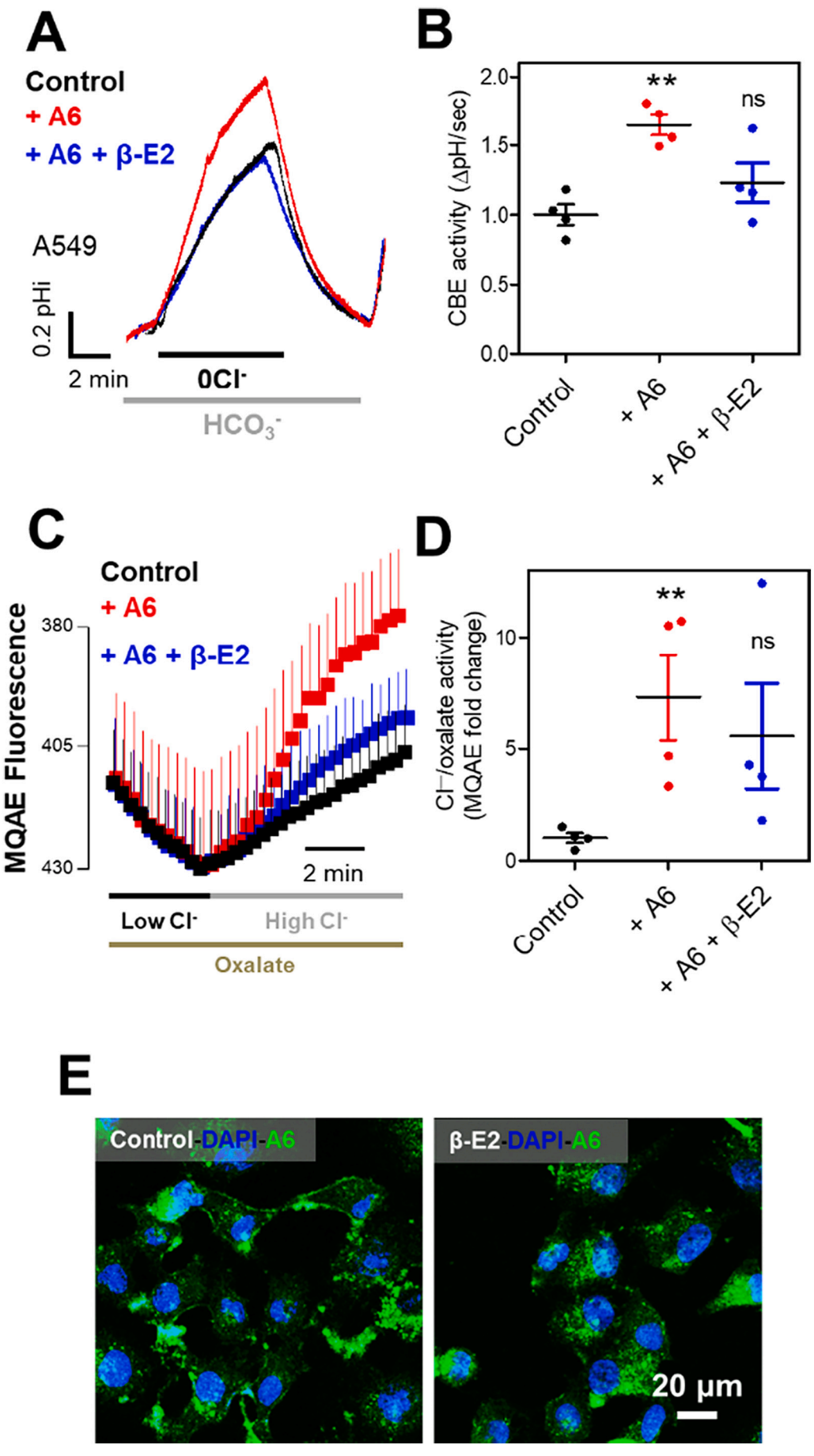

Fig. 6. β-E2 treatment attenuated the membrane expression and activity of A6. (A) Activity of CBE in A549 cells under the indicated conditions. (B) Graph shows means ± SEMs of relative CBE activities ($n = 4$, $^{**}p < 0.01$, ns = non-significant). (C) Activity of COE in A549 cells under the indicated conditions. (D) The graph shows means ± SEMs of relative COE activities (n = 4, $^{**}p < 0.01$, ns = non-significant). (E) Confocal microscopy images of A6 (A6, green)-transfected A549 cells treated with or without β-E2.

effect of β-E2.

3.5. NHE activity was independent of siA6- or β-E2 treatment –mediated migration

Cellular migration, especially cancer cell migration, favors to move toward acidic extracellular circumstances (Stock et al., 2005). Proton release by NHE causes acidification of the extracellular milieu, and coordinates acid-base homeostasis NBC (Akiba et al., 1987; Preisig and Alpern, 1988; Soleimani et al., 1992). In addition, NHE activity was reduced in the renal proximal tubules of *Slc26a6*-deleted mice (Petrovic et al., 2008). Accordingly, we examined the involvement of NHE and NBC activities under enhanced migratory conditions such as after *A6* knockdown and in the presence of β-E2 treatment. NHE activity was not altered by *A6* depletion (Fig. 5A,B) or by β-E2 treatment (Fig. 5C,D). Additionally, NBC activity was not altered by *A6* depletion (Fig. 5E,F) or by β-E2 treatment (Fig. 5G,H). These results indicate NHE and NBC activities are independent of *A6* deletion- or by β-E2 treatment-mediated cellular migration.

3.6. β-E2 treatment attenuated the membrane expression and activity of A6

We are still needed to obtain the direct evidence which verifies the role of β-E2 on A6-mediated CBE or COE activities. Native immunostaining of A6 in A549 cells failed because of no appropriate antibody of A6. Thus cells were overexpressed A6 to verify the effect of β-E2 on A6 in A549 cells. Treatment with β-E2 reduced CBE activity (Fig. 6A,B) and COE activity (Fig. 6C,D) in A6-overexpressed cells. In addition, β-E2 treatment reduced the membrane localization of A6 and increased its cytosolic localization (Fig. 6E). These results indicate that β-E2 treatment attenuates the membrane stability of A6 without changes of total protein expression level.

4. Discussion

In this study, we investigated the effect of estrogen on A6 activity in lung cancer cells. Although estrogen stimulation unaffected the expression of A6, bicarbonate or oxalate transporting activity of A6 was attenuated, whereas cellular migration was enhanced. The effects of *A6*-knockdown or co-expressed SPAK with A6 on cellular migration were in line with observations of reduced A6 membrane expression and transporter activity. However, these attenuated transporter activities enhanced cellular migration, and similarly, overexpression of A6 dramatically reduced cellular migration. It has been known that ion transporting activities of ion transporters such as sodium bicarbonate cotransporters are critical role in cellular migration (Hwang et al., 2020b; Schwab, 2001; Schwab and Stock, 2014). However, the existence of A6 toward cellular motility was revealed negative effect on cellular migration.

Although genetically no disease-related human mutation of *A6* has yet been discovered, the functional effects of A6 as a bicarbonate or oxalate transporter on mouse cardiac function during cardioplegic arrest (Ji et al., 2019), the mouse cardiac system (Sirish et al., 2017), and in various human diseases such as duodenal ulcer (Wen et al., 2018) and nephrolithiasis (Amin et al., 2018; Khamaysi et al., 2019; Ohana et al., 2013) have been established. The present study provided clues regarding the nature of the relation between attenuated A6 levels and nephrolithiasis. A6 is physically or structurally associated with cystic fibrosis transmembrane conductance regulator (CFTR) (Lohi et al., 2003; Wang et al., 2006). Moreover, in patients with cystic fibrosis, CFTR dysregulation was observed to be associated with enhanced oxaluria (Gibney and Goldfarb, 2003; Hoppe et al., 2005; Knauf et al., 2017). The present study shows that enhanced estrogen level attenuates oxalate or bicarbonate transporting activity through A6 in A549 lung cancer cells. A6 protein overexpression reduced cellular migration even in presence of estrogen. Although the mechanisms linking altered oxalate and calcium homeostasis and stone formation have not been determined in this study, our results suggest regulation of A6-mediated oxalate transporting activity may be an important component of the linkage with estrogen level even in lung cancer cells.

Although the relationship between cancer and kidney stone seems to be independent, it should be considered that enhanced cancer risk has been reported in patients with kidney stones (Shih et al., 2014) and reduced *Slc26a6* expression in *ob* mice induces oxaluria (Amin et al., 2018). We assumed that highly dominant A6-expressed cells such as salivary duct or kidney (Lee et al., 2012b; Lohi et al., 2003; Mukaibo et al., 2018; Wang et al., 2002) would be affected by the treatment of estrogen. Reduced oxalate transporting activity by estrogen might induce an imbalance of oxalate homeostasis in salivary glands or kidney, which is highly expressed A6 and affect secreted oxalate level (Jiang et al., 2006; Knauf et al., 2011; Ohana et al., 2013; Taher, 1989; Yamamoto et al., 1983). Reduced COE activity of A6 by estrogen as we addressed in this study might be a similar effect with *Slc26a6*-null mice, which is shown to the reduced-transcellular oxalate secretion (Knauf et al., 2011). Accordingly, its regulatory role of estrogen on A6 activity might arise additional effects on the regulation of transcellular oxalate secretion in salivary glands, intestines, or kidneys.

Various studies of relationship between hormone and renal stone formation have been elucidated. Low level of sex hormone estrogen is clinically associated with potential risk of renal stone formation (Heller et al., 2002; Nackeeran et al., 2021; Peerapen and Thongboonkerd, 2019), and postmenopausal women with low level of estrogen reveal the enhanced risk of renal stone formation (Dey et al., 2002; Maalouf et al., 2010). Males reveal higher incidence of renal stone than female (Gupta et al., 2016; Wang et al., 2021; Ziemba and Matlaga, 2017). Although its mechanism remains unknown, sex hormone signaling and hormone levels on life stage would be closely related with kidney stone formation. Thus, our results reflect that A6-expressed cells might reduce oxalate transport by estrogen stimulation and paradoxically might possess reduced incidence of oxalate crystal complex. Additionally, female hormone-regulated A6 activity may provide the evidence of modulating factor associated with oxalate-mediated stone formation in humans. Based on our results, HRT would possess beneficial effect against oxalate-mediated stone formation, whereas should be also considered the enhanced motility of cancer cells.

Funding

This research was funded by the National Research Foundation of Korea (NRF) funded by the Korean government (NRF-2020R1A4A1016029, PC-WL and 2020R1A2C2003409, DMS).

Author contributions

DL, PC-WL, and JHH conceptualized and designed the study and acquired, analyzed, and interpreted data; DL and JHH drafted the manuscript and acquired data. JHH and DMS revised the manuscript critically for important intellectual content; JHH, PC-WL, and DMS contributed to the funding acquisition and final approval of the published version and are responsible for all aspects of the work as regards the accuracy and integrity of the study.

Declaration of Competing Interest

The authors have no conflict of interest to declare.

Appendix A. Supplementary data

Supplementary data to this article can be found online at https://doi.org/10.1016/j.tiv.2022.105373.

References

Akiba, T., Rocco, V.K., Warnock, D.G., 1987. Parallel adaptation of the rabbit renal cortical sodium/proton antiporter and sodium/bicarbonate cotransporter in metabolic acidosis and alkalosis. J. Clin. Invest. 80, 308–315.

Alvarez, B.V., Kieller, D.M., Quon, A.L., Markovich, D., Casey, J.R., 2004. Slc26a6: a cardiac chloride-hydroxyl exchanger and predominant chloride-bicarbonate exchanger of the mouse heart. J. Physiol. 561, 721–734.

Amin, R., Asplin, J., Jung, D., Bashir, M., Alshaikh, A., Ratakonda, S., Sharma, S., Jeon, S., Granja, I., Matern, D., Hassan, H., 2018. Reduced active transcellular intestinal oxalate secretion contributes to the pathogenesis of obesity-associated hyperoxaluria. Kidney Int. 93, 1098–1107.

Celojevic, D., Petersen, A., Karlsson, J.O., Behndig, A., Zetterberg, M., 2011. Effects of 17beta-estradiol on proliferation, cell viability and intracellular redox status in native human lens epithelial cells. Mol. Vis. 17, 1987–1996.

Chakraborty, S., Ganti, A.K., Marr, A., Batra, S.K., 2010. Lung cancer in women: role of estrogens. Exp. Rev. Respir. Med. 4, 509–518.

Dawson-Hughes, B., Dallal, G.E., Krall, E.A., Sadowski, L., Sahyoun, N., Tannenbaum, S., 1990. A controlled trial of the effect of calcium supplementation on bone density in postmenopausal women. N. Engl. J. Med. 323, 878–883.

Dey, J., Creighton, A., Lindberg, J.S., Fuselier, H.A., Kok, D.J., Cole, F.E., Hamm, L., 2002. Estrogen replacement increased the citrate and calcium excretion rates in postmenopausal women with recurrent urolithiasis. J. Urol. 167, 169–171.

Domrongkitchaiporn, S., Ongphiphadhanakul, B., Stitchantrakul, W., Chansirikarn, S., Puavilai, G., Rajatanavin, R., 2002. Risk of calcium oxalate nephrolithiasis in postmenopausal women supplemented with calcium or combined calcium and estrogen. Maturitas 41, 149–156.

Evans, R.L., Turner, R.J., 1997. Upregulation of Na(+)-K(+)-2Cl- cotransporter activity in rat parotid acinar cells by muscarinic stimulation. J. Physiol. 499 (Pt 2), 351–359.

Fan, J., Chandhoke, P.S., Grampsas, S.A., 1999. Role of sex hormones in experimental calcium oxalate nephrolithiasis. J. Am. Soc. Nephrol. 10 (Suppl. 14), S376–S380.

Freel, R.W., Hatch, M., Green, M., Soleimani, M., 2006. Ileal oxalate absorption and urinary oxalate excretion are enhanced in Slc26a6 null mice. Am. J. Physiol. Gastrointest. Liver Physiol. 290, G719–G728.

Garcia-Perez, I., Villasenor, A., Wijeyesekera, A., Posma, J.M., Jiang, Z., Stamler, J., Aronson, P., Unwin, R., Barbas, C., Elliott, P., Nicholson, J., Holmes, E., 2012. Urinary metabolic phenotyping the slc26a6 (chloride-oxalate exchanger) null mouse model. J. Proteome Res. 11, 4425–4435.

Gibney, E.M., Goldfarb, D.S., 2003. The association of nephrolithiasis with cystic fibrosis. Am. J. Kidney Dis. 42, 1–11.

Gupta, K., Gill, G.S., Mahajan, R., 2016. Possible role of elevated serum testosterone in pathogenesis of renal stone formation. Int. J. Appl. Basic Med. Res. 6, 241–244.

Heller, H.J., Sakhaee, K., Moe, O.W., Pak, C.Y., 2002. Etiological role of estrogen status in renal stone formation. J. Urol. 168, 1923–1927.

Hong, J.H., Muhammad, E., Zheng, C., Hershkovitz, E., Alkrinawi, S., Loewenthal, N., Parvari, R., Muallem, S., 2015. Essential role of carbonic anhydrase XII in secretory gland fluid and HCO3 (−) secretion revealed by disease causing human mutation. J. Physiol. 593, 5299–5312.

Hoppe, B., von Unruh, G.E., Blank, G., Rietschel, E., Sidhu, H., Laube, N., Hesse, A., 2005. Absorptive hyperoxaluria leads to an increased risk for urolithiasis or nephrocalcinosis in cystic fibrosis. Am. J. Kidney Dis. 46, 440–445.

Hsu, L.H., Chu, N.M., Kao, S.H., 2017. Estrogen, estrogen receptor and lung cancer. Int. J. Mol. Sci. 18.

Hwang, S., Shin, D.M., Hong, J.H., 2019. Drug repurposing as an antitumor agent: disulfiram-mediated carbonic anhydrase 12 and anion exchanger 2 modulation to inhibit Cancer cell migration. Molecules 24.

Hwang, S., Shin, D.M., Hong, J.H., 2020a. Intracellular Ca2+−mediated AE2 is involved in the vectorial movement of HaCaT keratinocyte. Int. J. Mol. Sci. 21.

Hwang, S., Shin, D.M., Hong, J.H., 2020b. Protective role of IRBIT on sodium bicarbonate cotransporter-n1 for migratory Cancer cells. Pharmaceutics 12.

Hwang, S., Lee, P.C.W., Shin, D.M., Hong, J.H., 2021. Modulated start-up mode of Cancer cell migration through Spinophilin-tubular networks. Frontiers in Cell and Developmental Biology 9.

Ji, M., Park, C.K., Lee, J.W., Park, K.Y., Son, K.H., Hong, J.H., 2017. Two phase modulation of [formula: see text] entry and Cl(−)/[formula: see text] exchanger in submandibular glands cells by Dexmedetomidine. Front. Physiol. 8, 86.

Ji, M., In Lee, S., Lee, S.A., Son, K.H., Hong, J.H., 2019. Enhanced activity by NKCC1 and Slc26a6 mediates acidic pH and Cl(−) movement after Cardioplegia-induced arrest of db/db diabetic heart. Mediat. Inflamm. 2019, 7583760.

Jiang, Z., Asplin, J.R., Evan, A.P., Rajendran, V.M., Velazquez, H., Nottoli, T.P., Binder, H.J., Aronson, P.S., 2006. Calcium oxalate urolithiasis in mice lacking anion transporter Slc26a6. Nat. Genet. 38, 474–478.

Khamaysi, A., Anbtawee-Jomaa, S., Fremder, M., Eini-Rider, H., Shimshilashvili, L., Aharon, S., Aizenshtein, E., Shlomi, T., Noguchi, A., Springer, D., Moe, O.W., Shcheynikov, N., Muallem, S., Ohana, E., 2019. Systemic succinate homeostasis and local succinate signaling affect blood pressure and modify risks for calcium oxalate Lithogenesis. J. Am. Soc. Nephrol. 30 (3), 381–392.

Knauf, F., Ko, N., Jiang, Z., Robertson, W.G., Van Itallie, C.M., Anderson, J.M., Aronson, P.S., 2011. Net intestinal transport of oxalate reflects passive absorption and SLC26A6-mediated secretion. J. Am. Soc. Nephrol. 22, 2247–2255.

Knauf, F., Thomson, R.B., Heneghan, J.F., Jiang, Z., Adebamiro, A., Thomson, C.L., Barone, C., Asplin, J.R., Egan, M.E., Alper, S.L., Aronson, P.S., 2017. Loss of cystic fibrosis transmembrane regulator impairs intestinal oxalate secretion. J. Am. Soc. Nephrol. 28, 242–249.

Lee, M.G., Ohana, E., Park, H.W., Yang, D., Muallem, S., 2012a. Molecular mechanism of pancreatic and salivary gland fluid and Hco3- secretion. Physiol. Rev. 92, 39–74.

Lee, M.G., Ohana, E., Park, H.W., Yang, D., Muallem, S., 2012b. Molecular mechanism of pancreatic and salivary gland fluid and HCO3 secretion. Physiol. Rev. 92, 39–74.

Lee, D., Lee, S.A., Shin, D.M., Hong, J.H., 2018. Chloride influx of anion exchanger 2 was modulated by calcium-dependent Spinophilin in submandibular glands. Front. Physiol. 9.

Liang, J., Shang, Y., 2013. Estrogen and cancer. Annu. Rev. Physiol. 75, 225–240.

Lohi, H., Lamprecht, G., Markovich, D., Heil, A., Kujala, M., Seidler, U., Kere, J., 2003. Isoforms of SLC26A6 mediate anion transport and have functional PDZ interaction domains. Am. J. Phys. Cell Phys. 284, C769–C779.

Maalouf, N.M., Sato, A.H., Welch, B.J., Howard, B.V., Cochrane, B.B., Sakhaee, K., Robbins, J.A., 2010. Postmenopausal hormone use and the risk of nephrolithiasis: results from the Women's Health Initiative hormone therapy trials. Arch. Intern. Med. 170, 1678–1685.

Mount, D.B., Romero, M.F., 2004. The SLC26 gene family of multifunctional anion exchangers. Pflugers Arch. 447, 710–721.

Mukaibo, T., Munemasa, T., George, A.T., Tran, D.T., Gao, X., Herche, J.L., Masaki, C., Shull, G.E., Soleimani, M., Melvin, J.E., 2018. The apical anion exchanger Slc26a6 promotes oxalate secretion by murine submandibular gland acinar cells. J. Biol. Chem. 293, 6259–6268.

Nackeeran, S., Katz, J., Ramasamy, R., Marcovich, R., 2021. Association between sex hormones and kidney stones: analysis of the National Health and nutrition examination survey. World J. Urol. 39, 1269–1275.

Ohana, E., Shcheynikov, N., Moe, O.W., Muallem, S., 2013. SLC26A6 and NaDC-1 transporters interact to regulate oxalate and citrate homeostasis. J. Am. Soc. Nephrol. 24, 1617–1626.

Peerapen, P., Thongboonkerd, V., 2019. Protective cellular mechanism of estrogen against kidney stone formation: a proteomics approach and functional validation. Proteomics 19, e1900095.

Petrovic, S., Barone, S., Wang, Z., McDonough, A.A., Amlal, H., Soleimani, M., 2008. Slc26a6 (PAT1) deletion downregulates the apical Na+/H+ exchanger in the straight segment of the proximal tubule. Am. J. Nephrol. 28, 330–338.

Preisig, P.A., Alpern, R.J., 1988. Chronic metabolic acidosis causes an adaptation in the apical membrane Na/H antiporter and basolateral membrane Na(HCO3)3 symporter in the rat proximal convoluted tubule. J. Clin. Invest. 82, 1445–1453.

Rodriguez-Lara, V., Ignacio, G.S., Cerbon Cervantes, M.A., 2017. Estrogen induces CXCR4 overexpression and CXCR4/CXL12 pathway activation in lung adenocarcinoma cells in vitro. Endocr. Res. 42, 219–231.

Rodriguez-Lara, V., Hernandez-Martinez, J.M., Arrieta, O., 2018. Influence of estrogen in non-small cell lung cancer and its clinical implications. J. Thorac. Dis. 10, 482–497.

Rothenberger, N.J., Somasundaram, A., Stabile, L.P., 2018. The role of the estrogen pathway in the tumor microenvironment. Int. J. Mol. Sci. 19.

Schwab, A., 2001. Ion channels and transporters on the move. News Physiol. Sci. 16, 29–33.

Schwab, A., Stock, C., 2014. Ion channels and transporters in tumour cell migration and invasion. Philos. Trans. R. Soc. Lond. Ser. B Biol. Sci. 369, 20130102.

Schwab, A., Fabian, A., Hanley, P.J., Stock, C., 2012. Role of ion channels and transporters in cell migration. Physiol. Rev. 92, 1865–1913.

Shih, C.J., Chen, Y.T., Ou, S.M., Yang, W.C., Chen, T.J., Tarng, D.C., 2014. Urinary calculi and risk of cancer: a nationwide population-based study. Medicine (Baltimore) 93, e342.

Singh, A.K., Sjoblom, M., Zheng, W., Krabbenhoft, A., Riederer, B., Rausch, B., Manns, M. P., Soleimani, M., Seidler, U., 2008. CFTR and its key role in in vivo resting and luminal acid-induced duodenal HCO3- secretion. Acta Physiol (Oxford) 193, 357–365.

Sirish, P., Ledford, H.A., Timofeyev, V., Thai, P.N., Ren, L., Kim, H.J., Park, S., Lee, J.H., Dai, G., Moshref, M., Sihn, C.R., Chen, W.C., Timofeyeva, M.V., Jian, Z., Shimkunas, R., Izu, L.T., Chiamvimonvat, N., Chen-Izu, Y., Yamoah, E.N., Zhang, X. D., 2017. Action potential shortening and impairment of cardiac function by ablation of Slc26a6. Circ. Arrhythm. Electrophysiol. 10.

Soleimani, M., Bizal, G.L., McKinney, T.D., Hattabaugh, Y.J., 1992. Effect of in vitro metabolic acidosis on luminal Na+/H+ exchange and basolateral Na+:HCO3- cotransport in rabbit kidney proximal tubules. J. Clin. Invest. 90, 211–218.

Stock, C., Gassner, B., Hauck, C.R., Arnold, H., Mally, S., Eble, J.A., Dieterich, P., Schwab, A., 2005. Migration of human melanoma cells depends on extracellular pH and Na+/H+ exchange. J. Physiol. 567, 225–238.

Stoletov, K., Beatty, P.H., Lewis, J.D., 2020. Novel therapeutic targets for cancer metastasis. Expert. Rev. Anticancer. Ther. 20, 97–109.

Taher, A.A., 1989. The incidence and composition of salivary stones (sialolithiasis) in Iran: analysis of 95 cases–a short report. Singap. Dent. J. 14, 33–35.

Thomson, R.B., Thomson, C.L., Aronson, P.S., 2016. N-glycosylation critically regulates function of oxalate transporter SLC26A6. Am. J. Phys. Cell Phys. 311, C866–C873.

van Hoof, H.J., van der Mooren, M.J., Swinkels, L.M., Rolland, R., Benraad, T.J., 1994. Hormone replacement therapy increases serum 1,25-dihydroxyvitamin D: a 2-year prospective study. Calcif. Tissue Int. 55, 417–419.

Vinader, V., Al-Saraireh, Y., Wiggins, H.L., Rappoport, J.Z., Shnyder, S.D., Patterson, L. H., Afarinkia, K., 2011. An agarose spot chemotaxis assay for chemokine receptor antagonists. J. Pharmacol. Toxicol. Methods 64, 213–216.

Wang, Z.H., Petrovic, S., Mann, E., Soleimani, M., 2002. Identification of an apical cl-/HCO3- exchanger in the small intestine. Am. J. Physiol. Gastrointest. Liver Physiol. 282, G573–G579.

Wang, Z., Wang, T., Petrovic, S., Tuo, B., Riederer, B., Barone, S., Lorenz, J.N., Seidler, U., Aronson, P.S., Soleimani, M., 2005. Renal and intestinal transport defects in Slc26a6-null mice. Am. J. Phys. Cell Phys. 288, C957–C965.

Wang, Y., Soyombo, A.A., Shcheynikov, N., Zeng, W., Dorwart, M., Marino, C.R., Thomas, P.J., Muallem, S., 2006. Slc26a6 regulates CFTR activity in vivo to

determine pancreatic duct HCO3- secretion: relevance to cystic fibrosis. EMBO J. 25, 5049–5057.
Wang, J., Wang, W., Wang, H., Tuo, B., 2020. Physiological and pathological functions of SLC26A6. Front. Med. (Lausanne) 7, 618256.
Wang, Z., Zhang, Y., Zhang, J., Deng, Q., Liang, H., 2021. Recent advances on the mechanisms of kidney stone formation (review). Int. J. Mol. Med. 48.
Wen, G., Deng, S., Song, W., Jin, H., Xu, J., Liu, X., Xie, R., Song, P., Tuo, B., 2018. *Helicobacter pylori* infection downregulates duodenal CFTR and SLC26A6 expressions through TGFbeta signaling pathway. BMC Microbiol. 18, 87.
Wiggins, H., Rappoport, J., 2010. An agarose spot assay for chemotactic invasion. Biotechniques 48, 121–124.
Worrell, R.T., Oghene, J., Matthews, J.B., 2004. Ammonium effects on colonic cl-secretion: anomalous mole fraction behavior. Am. J. Physiol. Gastrointest. Liver Physiol. 286, G14–G22.
Yamamoto, H., Sakae, T., Takagi, M., Otake, S., Hirai, G., 1983. Weddellite in submandibular gland calculus. J. Dent. Res. 62, 16–19.
Zhu, Y., Huang, Y., Chen, L., Guo, L., Wang, L., Li, M., Liang, Y., 2021. Up-regulation of SLC26A6 in hepatocellular carcinoma and its diagnostic and prognostic significance. Crit. Rev. Eukaryot. Gene Expr. 31, 79–94.
Ziemba, J.B., Matlaga, B.R., 2017. Epidemiology and economics of nephrolithiasis. Investig. Clin. Urol. 58, 299–306.